Appl. Phys. A 63, 109–115 (1996)

Applied Physics A Materials Science & Processing

Femtosecond, picosecond and nanosecond laser ablation of solids

B.N. Chichkov, C. Momma, S. Nolte, F. von Alvensleben, A. Tünnermann

Laser Zentrum Hannover e.V., Hollerithallee 8, D-30419 Hannover, Germany
(Fax: + 49-511/2788-100)

Received: 23 February 1996/Accepted: 27 February 1996

Abstract. Laser ablation of solid targets by 0.2–5000 ps Ti:Sapphire laser pulses is studied. Theoretical models and qualitative explanations of experimental results are presented. Advantages of femtosecond lasers for precise material processing are discussed and demonstrated.

PACS: 81.15

Efficient use of lasers for precise material processing is impossible without a thorough knowledge of the fundamental laws governing the interaction of laser radiation with matter. For this goal systematic studies of the laser-matter interaction are necessary. Due to the recent progress of laser systems, especially those based on the chirped pulse amplification (CPA) technique, such systematic studies have become possible in a very broad range of laser parameters. With CPA systems the laser pulse duration can be varied from about one hundred femtoseconds to several nanoseconds leaving other laser parameters unchanged. This allows to perform a very detailed analysis of different nonstationary laser-matter interaction processes. As an example, recent investigations of the damage threshold [1], of the ablation threshold [2], and of the high-intensity laser ablation [3] can be mentioned. Note that such systematic studies have just begun, much more should be done for the understanding and demonstration of the potential of femtosecond laser systems for precise material processing.

Recently several experiments [4–6] comparing laser ablation of solid targets by femtosecond and nanosecond pulses have been performed. In [4] and [5, 6] advantages of femtosecond lasers for precise material processing with dye and excimer laser systems have been demonstrated. In this paper, we present our results on ablation and hole drilling with a commercial, 10 Hz, femtosecond Ti:Sapphire laser system which provides laser pulses at 780 nm with a pulse energy of up to 100 mJ and a variable pulse duration in the range of 0.2 to 5000 ps. Experiments are performed in a low fluence regime, slightly above the evaporation threshold. This regime is most interesting for precise material processing, since in this case the energy deposited into the solid and the heat-affected zones are minimized. We discuss and demonstrate advantages of the femtosecond-pulse lasers. We hope that our results can stimulate new investigations in this field. In Sect. 1, characteristic features of the low fluence laser ablation of metal targets in three different pulse duration regimes: femtosecond, picosecond and nanosecond are considered. The experimental setup and results are presented in Sect. 2.

1 Theoretical background

During the interaction of low intensity short laser pulses with metal targets the laser energy is absorbed by free electrons, due to the inverse Bremsstrahlung. Then the evolution of the absorbed laser energy involves thermalization within the electron subsystem, energy transfer to the lattice, and energy losses due to the electron heat transport into the target. If we assume that the thermalization within the electron subsystem is very fast and that the electron and the lattice subsystems can be characterized by their temperatures (T_e and T_i), the energy transport into the metal can be described by the following one-dimensional, two-temperature diffusion model [7, 8]:

$$C_e \frac{\partial T_e}{\partial t} = -\frac{\partial Q(z)}{\partial z} - \gamma(T_e - T_i) + S, \tag{1}$$

$$C_i \frac{\partial T_i}{\partial t} = \gamma(T_e - T_i), \tag{2}$$

$$Q(z) = -k_e \partial T_e / \partial z, \quad S = I(t) A\alpha \exp(-\alpha z). \tag{3}$$

Here z is the direction perpendicular to the target surface, $Q(z)$ is the heat flux, S is the laser heating source term, $I(t)$ is the laser intensity, $A = 1 - R$ and α are the surface transmissivity and the material absorption coefficient, C_e and C_i are the heat capacities (per unit volume) of the electron and lattice subsystems, γ is the parameter characterizing the electron-lattice coupling, k_e is the electron

thermal conductivity. In the above equations a thermal conductivity in the lattice subsystem (phonon component) is neglected. The electronic heat capacity is much less than the lattice heat capacity, therefore electrons can be heated to very high transient temperatures. When the electron temperature (in units of energy) remains smaller than the Fermi energy, the electron heat capacity and the nonequilibrium electron thermal conductivity are given by $C_e = C'_e T_e$ (where C'_e is a constant) and $k_e = k_0(T_i) \cdot T_e/T_i$ (where $k_0(T_i)$ is the conventional equilibrium thermal conductivity of a metal) [9–11]. Expressions for the coupling constant γ are given in [7, 12] and results of recent measurements in [11, 13, 14].

Equations (1–3) have three characteristic time scales τ_e, τ_i and τ_L, where $\tau_e = C_e/\gamma$ is the electron cooling time, $\tau_i = C_i/\gamma$ is the lattice heating time ($\tau_e \ll \tau_i$) and τ_L is the duration of the laser pulse. These parameters define three different regimes of the laser-metal interaction which we call femtosecond, picosecond and nanosecond regimes.

Femtosecond pulses

First we consider the case when the laser pulse duration is shorter than the electron cooling time, $\tau_L \ll \tau_e$. For $t \ll \tau_e$, which is equivalent to $C_e T_e/t \gg \gamma T_e$, the electron-lattice coupling can be neglected. In this case (1) can be easily solved. Since the general solution of this equation is quite complicated, we neglect the electron heat conduction term in our formulas. This can be done when the following condition is fulfilled $D_e \tau_L < \alpha^{-2}$, where $D_e = k_e/C_e$ is the electron thermal diffusivity. In this case (1) reduces to

$$C'_e \partial T_e^2/\partial t = 2 I_a \alpha \exp(-\alpha z) \tag{4}$$

and gives

$$T_e(t) = \left(T_0^2 + \frac{2 I_a \alpha}{C'_e} t \exp(-\alpha z) \right)^{1/2}. \tag{5}$$

Here $I(t) = I_0$ is assumed constant, $I_a = I_0 A$, and $T_0 = T_e(0)$ is the initial temperature. At the end of the laser pulse the electron temperature is given by

$$T_e(\tau_L) \simeq \left(\frac{2 F_a \alpha}{C'_e} \right)^{1/2} \exp(-z/\delta), \tag{6}$$

where $T_e(\tau_L) \gg T_0$ is assumed, $F_a = I_a \tau_L$ is the absorbed laser fluence, and $\delta = 2/\alpha$ is the skin depth.

The evolution of the electron and lattice temperatures after the laser pulse is described by (1–3) with $S = 0$. Initial conditions for the electron and lattice temperatures are given by (6) and $T_i = T_0$. After the laser pulse the electrons are rapidly cooled due to the energy transfer to the lattice and heat conduction into the bulk. Since this electron cooling time is very short, (2) can be written as $T_i \simeq T_e(\tau_L)\ t/\tau_i$ (here the initial lattice temperature is neglected). The attainable lattice temperature is determined by the average cooling time of the electrons $\tau_e^a = C'_e T_e(\tau_L)/2\gamma$ and is given by

$$T_i \simeq T_e^2(\tau_L) \frac{C'_e}{2 C_i} \simeq \frac{F_a \alpha}{C_i} \exp(-\alpha z). \tag{7}$$

Note that the problem of the hot electron relaxation dynamics in metals after the excitation by a femtosecond laser pulse has been intensively studied during the last years [14–16]. It has been shown that the time scale for the fast electron cooling and a considerable energy transfer to the lattice is of the order of 1 ps.

The significant evaporation occurs when $C_i T_i$ becomes larger than $\rho\Omega$, where ρ is the density and Ω is the specific (per unit mass) heat of evaporation. Using (7), we can write the condition for strong evaporation in the form

$$F_a \geq F_{th} \exp(\alpha z), \tag{8}$$

where $F_{th} \simeq \rho\Omega/\alpha$ is the threshold laser fluence for evaporation with femtosecond pulses. Then the ablation depth per pulse L is

$$L \simeq \alpha^{-1} \ln(F_a/F_{th}). \tag{9}$$

The logarithmic dependence of the ablation depth on the laser pulse fluence is well known for the laser ablation of organic polymers. Recently the logarithmic dependence of the ablation depth per pulse has been demonstrated for metal targets with femtosecond KrF-laser pulses [5].

Due to the very short time scales involved in the ablation with femtosecond laser pulses the ablation process can be considered as a direct solid-vapor (or solid-plasma) transition. In this case the lattice is heated on a picosecond time scale which results in the creation of vapor and plasma phases followed by a rapid expansion in vacuum. During all these processes thermal conduction into the target can be neglected in a first approximation. These advantages of femtosecond laser pulses allow very precise and pure laser-processing of metals (and other solids) which is experimentally demonstrated below.

Picosecond pulses

Now we turn to the discussion of ablation with picosecond laser pulses when the following condition is fulfilled $\tau_e \ll \tau_L \ll \tau_i$.

At a time $t \gg \tau_e$ which is equivalent to $C_e T_e/t \ll \gamma T_e$, (1) for the electron temperature becomes quasistationary, and (1–3) reduce to

$$\partial/\partial z (k_e \partial T_e/\partial z) - \gamma(T_e - T_i) + I_a \alpha \exp(-\alpha z) = 0, \tag{10}$$

$$T_i = \frac{1}{\tau_i} \int_0^t \exp\left(-\frac{t-\theta}{\tau_i} \right) T_e(\theta)\, d\theta + T_0. \tag{11}$$

Here (2) for the lattice temperature is written in the integral form. These equations describe heating of metal targets by the laser pulses with $\tau_L \gg \tau_e$. When the condition $t \ll \tau_i$ is fulfilled, (11) can be simplified due to the quasistationary character of the electron temperature. Neglecting T_0, we get

$$T_i \simeq T_e(1 - \exp(-t/\tau_i)) \simeq (t/\tau_i) T_e. \tag{12}$$

As can be seen from this expression, in the picosecond regime the lattice temperature remains much less than the

electron temperature. This allows to neglect the lattice temperature in (10). The analysis of (10, 12) is especially simple when the condition $k_e T_e \alpha^2 \ll \gamma T_e$ is fulfilled. In this case the electron cooling is due to the energy exchange with the lattice. The electron temperature and the lattice temperature at the end of the laser pulse are given by

$$T_e \simeq \frac{I_a \alpha}{\gamma} \exp(-\alpha z), \quad T_i \simeq \frac{F_a \alpha}{C_i} \exp(-\alpha z). \tag{13}$$

Note that the attainable lattice temperature after the laser pulse is again determined by the electron cooling time. Since $\tau_e \ll \tau_L$, the attainable lattice temperature and the lattice temperature at the end of the laser pulse are approximately equal. In femtosecond and picosecond regimes (7) and (13) give the same expressions for the lattice temperature. Therefore, the condition for strong evaporation given by (8), the fluence threshold and the ablation depth per pulse given by (9) remain unchanged.

Thus, the logarithmic dependence of the ablation depth on the laser pulse fluence is also possible in the picosecond range. In our derivations we have neglected the electron heat conduction into the target. This is a very crude assumption for the description of laser ablation of metal targets in the picosecond regime. Laser ablation in this case is accompanied by the electron heat conduction and formation of a melted zone inside the target. In spite that at the surface we can again consider evaporation as a direct solid-vapor (or solid-plasma) transition, the presence of the liquid phase inside the target reduces the precision of laser processing of metals in this regime (see below).

Nanosecond pulses

Here we briefly discuss ablation with nanosecond laser pulses when the condition $\tau_L \gg \tau_i$ is fulfilled. In this case the electron and lattice temperatures are equal $T_e = T_i = T$, and (1–3) reduce to

$$C_i \partial T/\partial t = \partial/\partial z (k_0 \partial T/\partial z) + I_a \alpha \exp(-\alpha z). \tag{14}$$

Laser heating of metal targets by long laser pulses has been a subject of many experimental and theoretical studies [17–20]. In this regime the absorbed laser energy first heats the target surface to the melting point and then to the vaporization temperature. Note that metals need much more energy to vaporize than to melt. During the interaction the main source of energy losses is the heat conduction into the solid target. The heat penetration depth is given by $l \sim (Dt)^{1/2}$, where D is the heat diffusion coefficient, $D = k_0/C_i$. Note that for long-pulse laser ablation of metal targets the condition $D\tau_L \alpha^2 \gg 1$ is usually fulfilled. The energy deposited inside the target per unit mass is given by $E_m \sim I_a t/\rho l$. When at a certain moment $t = t_{th}$ this energy becomes larger than the specific heat of evaporation Ω, significant evaporation occurs. From the condition $E_m \sim \Omega$ we get $t_{th} \sim D(\Omega \rho / I)^2$ (see [17]). Thus, the condition for strong evaporation, $E_m > \Omega$ (or $\tau_L > t_{th}$), can be written as

$$I > I_{th} \sim \frac{\rho \Omega D^{1/2}}{\tau_L^{1/2}}, \quad F > F_{th} \sim \rho \Omega D^{1/2} \times \tau_L^{1/2} \tag{15}$$

for laser intensity and fluence, respectively. The threshold laser fluence which is necessary for evaporation with long laser pulses grows as $\tau_L^{1/2}$.

In case of ablation with long laser pulses there is enough time for the thermal wave to propagate into the target and to create a relatively large layer of melted material. In this case the evaporation occurs from the liquid metal, which makes precise material processing of metal targets in vacuum with nanosecond pulses very complicated.

2 Experimental setup and results

Now we turn to the discussion of experimental results on a low fluence laser ablation of metals and other solids. In our experiments a commercial femtosecond Ti:Sapphire laser system (BMI Alpha 10A) based on the chirped-pulse amplification (CPA) technique [21] is used. A detailed description of the principal setup is given in [22]. This system provides laser pulses at 780 nm with a variable pulse energy of up to 100 mJ. Due to the CPA technique the pulse duration can be varied from 200 fs up to 400 ps. In this pulse duration range the spectral pulse width remains constant (approximately 8 nm). Pulse duration measurements for pulses shorter than 10 ps are performed by a background free second order autocorrelator and for pulses longer than 10 ps by a picosecond streak camera (Hadland, IMACON 500). Pulse widths of 3–5 ns are obtained when the regenerative amplifier (see [22]) is not seeded by the femtosecond oscillator (Coherent, Mira Basic). In this case the regenerative amplifier operates as an oscillator, and the spectral width of the generated pulses is significantly reduced. The time durations of the nanosecond pulses have been measured by a photodiode in combination with a fast sampling oscillograph and by the streak camera.

Our experiments are performed in the low fluence regime ($F = 0.1$–$5\ \mathrm{J/cm^2}$) with an imaging geometry. An aperture ($d = 5$ mm), mounted in the beam pass, is imaged (with demagnification factor of $\simeq 1/30$) onto the target surface by a $f = 140$ mm suprasil lense. The laser beam diameter is approximately 20 mm. As target materials steel, copper, AlN and silicon plates are used. These plates are attached to a computer controlled x,y,z-translation stage which is mounted in a vacuum cell at a pressure below 10^{-4} mbar. The number of pulses which are necessary to drill through the target plate is controlled by a photodiode mounted behind the targets.

First we present our results on the laser processing of metal targets. We compare holes drilled in 100 μm thick steel foils (in vacuum) with 10^4 laser pulses in three different regimes: femtosecond, picosecond and nanosecond. In Fig. 1 schematic of femtosecond-pulse laser ablation and the hole drilled with 200 fs, 120 μJ, $F = 0.5\ \mathrm{J/cm^2}$ laser pulses are shown. As can be seen, there is no trace of the molten material. Only a vapor dust ring around the hole.

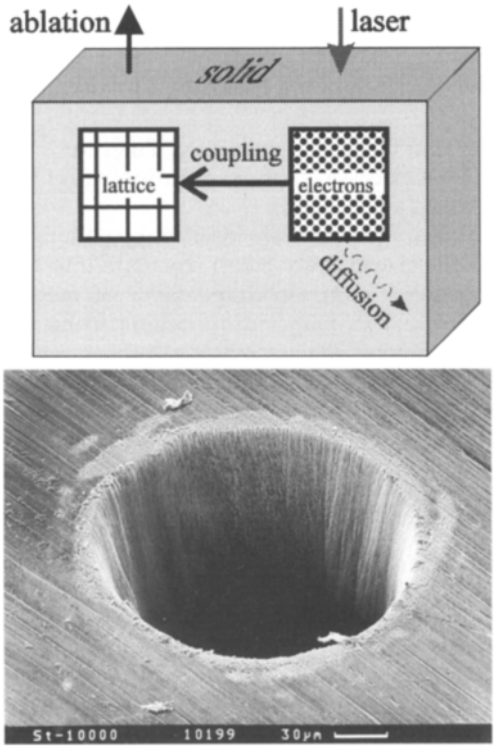

Fig. 1. Schematic of femtosecond-pulse laser ablation and a SEM photograph of a hole drilled in a 100 μm thick steel foil with 200 fs, 120 μJ, $F = 0.5$ J/cm^2 laser pulses at 780 nm

In Fig. 2 schematic of nanosecond-pulse laser ablation and the holes drilled with (a) 80 ps, 900 μJ, $F = 3.7$ J/cm^2; and (b) 3.3 ns, 1 mJ, and $F = 4.2$ J/cm^2 laser pulses are shown. The trace of the molten material can be seen in these figures. The presence of liquid phase leads to an unstable drilling process (see Fig. 2a). In case of ablation with nanosecond pulses there is enough time for the thermal wave to propagate into the metal target and to create a relatively large molten layer. In this case the target material is removed both in vapor and liquid phases, since the vaporization process creates a recoil pressure that expels the liquid. In Fig. 2b a "corona" created due to the recoil vapor pressure is clearly seen. Note that these are the best results which we obtain with 80 ps and 3.3 ns laser pulses at fluences as low as possible. When the laser fluence is reduced further the drilling through the 100 μm steel plate in vacuum becomes impossible.

Comparing Fig. 1 and Fig. 2, the advantages of femtosecond-pulse lasers for precise material processing become evident. Moreover, due to the absence of thermal losses in the femtosecond regime, holes in metal targets can be drilled with much lower laser fluences.

Below we present additional illustrative information on femtosecond-pulse laser ablation of different targets with the second harmonic of Ti:Sapphire laser radiation ($\lambda = 390$). The second harmonic is used to minimize diffraction effects and to improve the quality of image projection. In Fig. 3 the development of the ablation process with the increasing number of 250 fs, 0.5 mJ, and $F = 2.5$ J/cm^2 laser pulses a) 10, b) 100, c) 10^3 and d) 5×10^3 is shown. The target is a 0.5 mm steel plate. In Fig. 3c the creation of characteristic structures is clearly seen. These structures appear due to the instability of a plane evaporation front [23].

In Fig. 4 the evolution of femtosecond-pulse laser ablation of a 1 mm thick copper target is shown with: a) 10, b) 100, c) 10^3, and d) 3×10^4 pulses. In Fig. 5

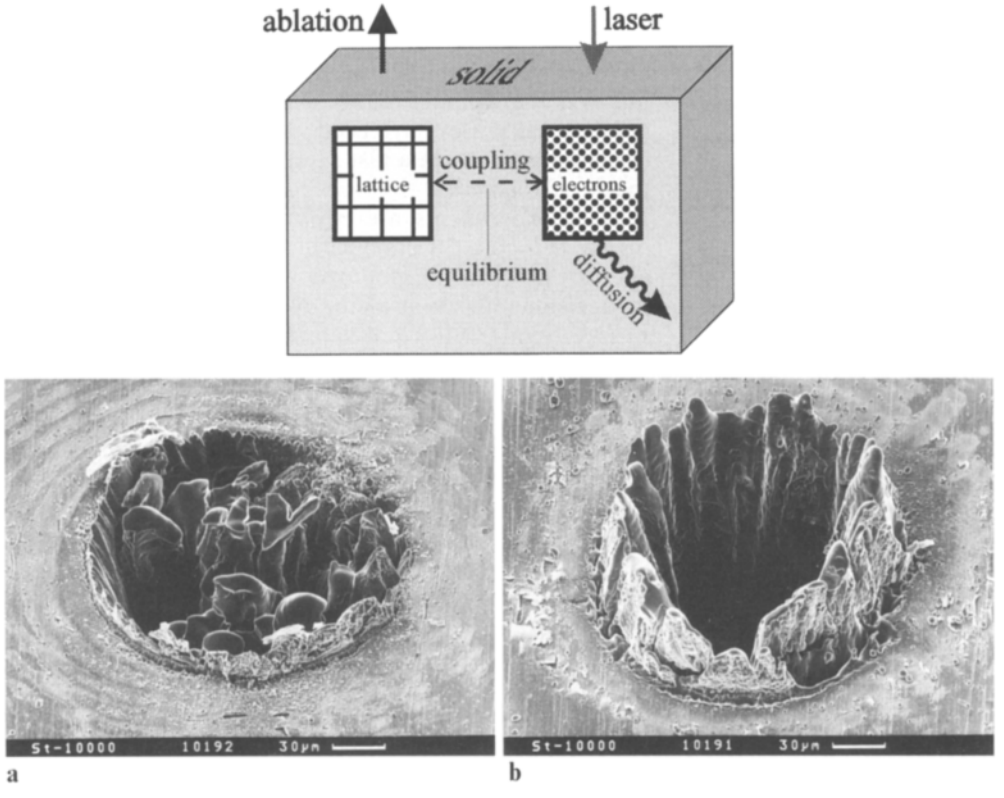

Fig. 2a, b. Schematic of nanosecond-pulse laser ablation and holes drilled in a 100 μm thick steel foil with **(a)** 80 ps, 900 μJ, $F = 3.7$ J/cm^2; and **(b)** 3.3 ns, 1 mJ, and $F = 4.2$ J/cm^2 laser pulses at 780 nm

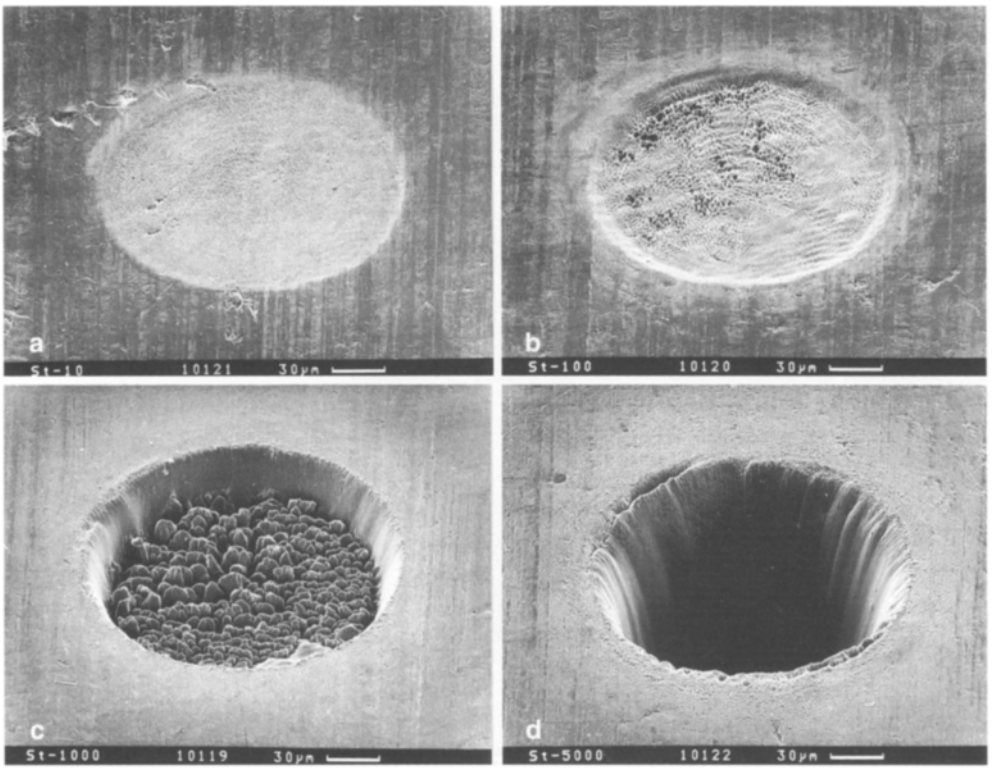

Fig. 3a–d. Femtosecond-pulse laser processing of a 0.5 mm steel plate with 250 fs, 0.5 mJ, and $F = 2.5\ \mathrm{J/cm^2}$ second harmonic radiation ($\lambda = 390$ nm) and different number of pulses: (**a**) 10, (**b**) 100, (**c**) 1000 and (**d**) 5000 laser pulses

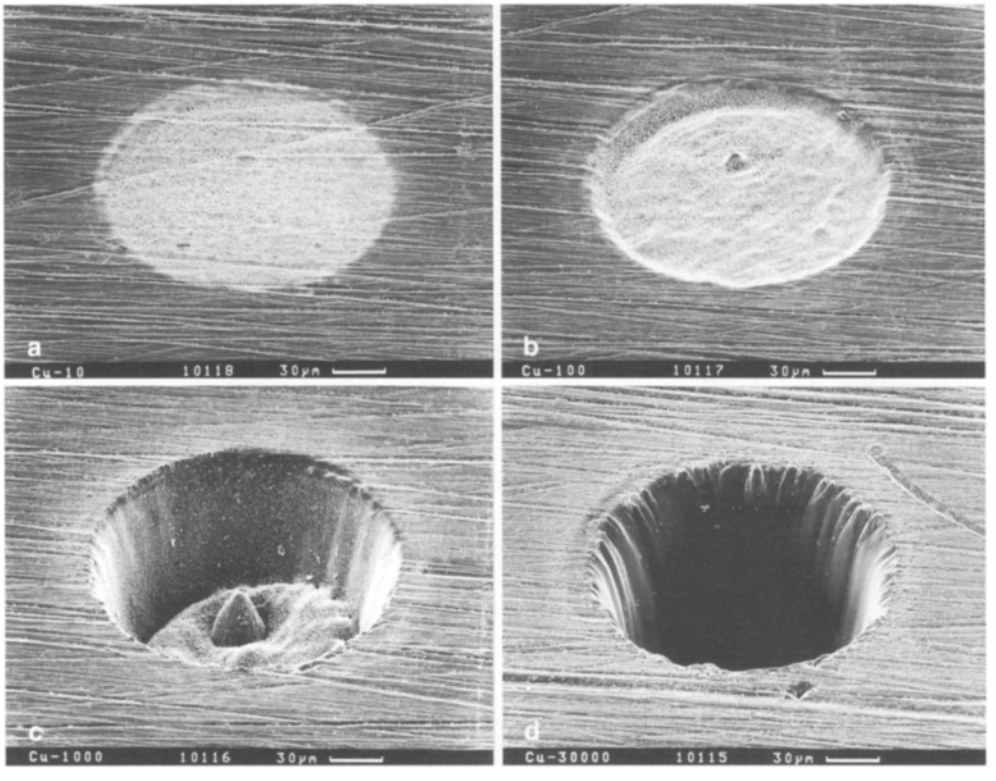

Fig. 4a–d. Evolution of femtosecond-pulse laser ablation of a 1 mm thick copper target with: (**a**) 10, (**b**) 100, (**c**) 10^3, and (**d**) 3×10^4 pulses. Laser parameters are the same as in Fig. 3

results of laser ablation of a 0.3 mm thick silicon target are demonstrated with: a) 10, b) 100, c) 5×10^3, and d) 10^4 pulses. Redeposition of the ablated material on the target surface is much stronger than in the case of metal targets. In Fig. 6 the ablation of a 0.8 mm AlN target with: a) 10, b) 10^3, and c) 3.5×10^4 laser pulses is illustrated. The laser parameters in Figs. 4, 5 and 6 are approximately the same as in Fig. 3.

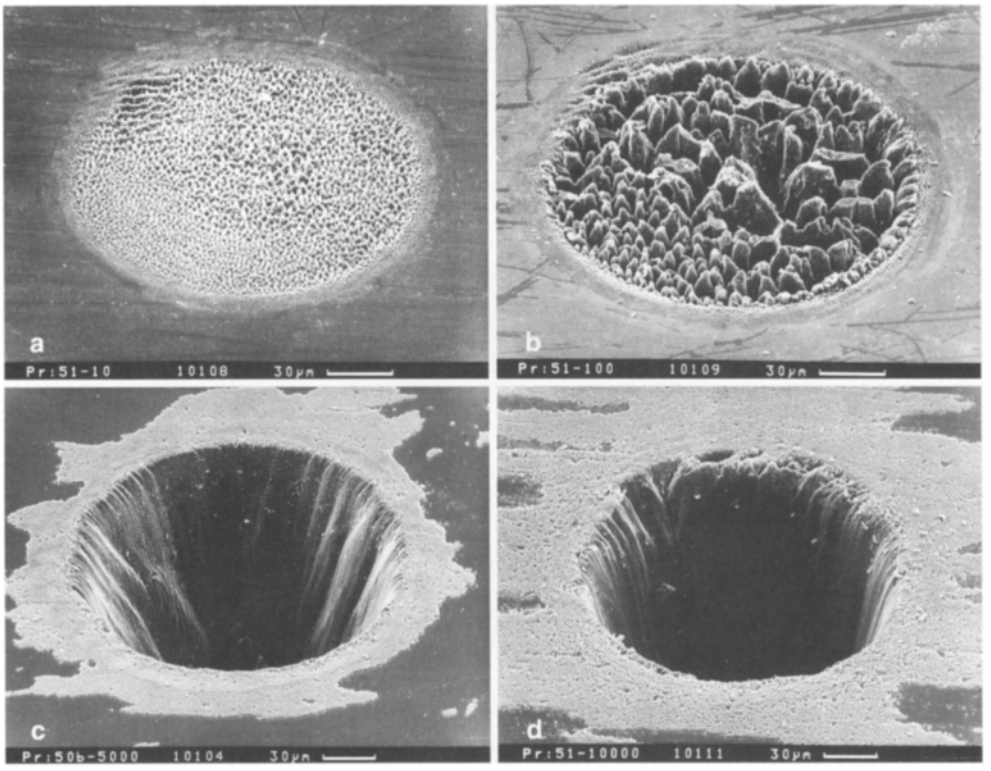

Fig. 5a–d. Laser ablation of a 0.3 mm thick silicon target with: (**a**) 10, (**b**) 100, (**c**) 5×10^3, and (**d**) 10^4 pulses. Laser parameters are the same as in Fig. 3

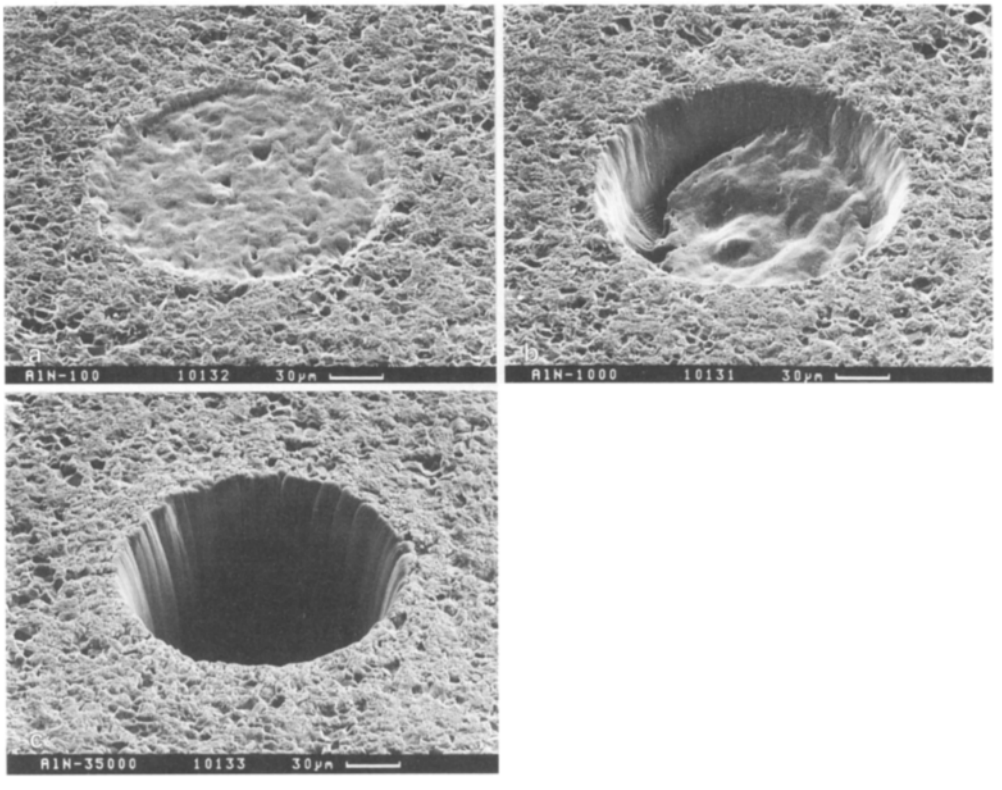

Fig. 6a–c. Ablation of a 0.8 mm AlN target with: (**a**) 10, (**b**) 10^3, and (**c**) 3.5×10^4 laser pulses. Laser parameters are approximately the same as in Fig. 3

Closing this section we summarize the main features of femtosecond laser material processing: very rapid creation of vapor and plasma phases, negligible heat conduction and the absence of liquid phase. The absence of the liquid phase allows better control during the drilling process. Therefore, the reproducibility of our results with femtosecond laser pulses is very good.

3 Conclusion

Theoretical models and experimental results on femtosecond, picosecond and nanosecond laser ablation of metal targets are presented. Very pure ablation of metal targets in vacuum with femtosecond laser pulses is demonstrated. Sharp well defined patterns can be ablated in metal and other solid targets by an image projection technique. These advantages of femtosecond lasers are very promising for their future applications in precise material processing.

Acknowledgements. We would like to thank Hanna Jacobs for technical assistance and acknowledge financial support by the German Ministry of Science, Education, Research, and Technology (BMBF, 13N6590/0).

References

1. B.C. Stuart, M.D. Feit, A.M. Rubenchik, B.W. Shore, M.D. Perry: Phys. Rev. Lett. **74**, 2248 (1995)
2. P.P. Pronko, S.K. Dutta, D. Du, R.K. Singh: J. Appl. Phys. **78**, 6233 (1995)
3. C. Momma, B.N. Chichkov, S. Nolte, F. von Alvensleben, A. Tünnermann, H. Welling: Opt. Commun. accepted
4. W. Kautek, J. Krüger: SPIE Proc. **2207**, 600 (1994)
5. S. Preuss, A. Demchuk, M. Stuke: Appl. Phys. A **61**, 33 (1995)
6. J. Ihlemann, A. Scholl, H. Schmidt, B. Wolff-Rottke: Appl. Phys. A **60**, 411 (1995)
7. M.I. Kaganov, I.M. Lifshitz, L.V. Tanatarov: Sov. Phys. –JETP **4**, 173 (1957)
8. S.I. Anisimov, B.L. Kapeliovich, T.L. Perel'man: Sov. Phys. –JETP **39**, 375 (1974)
9. M.B. Agranat, A.A. Benditskii, G.M. Gandel'man, P.S. Kondratenko, B.I. Makshantsev, G.I. Rukman, B.M. Stepanov: Sov. Phys. –JETP **52**, 27 (1980)
10. M.B. Agranat, S.I. Anisimov, S.I. Ashitkov, B.I. Makshantsev, I.B. Ovchinnikova: Sov. Phys. –Solid State **29**, 1875 (1987)
11. P.B. Corkum, F. Brunel, N.K. Sherman, T. Srinivasan-Rao: Phys. Rev. Lett. **61**, 2886 (1988)
12. P.B. Allen: Phys. Rev. Lett. **59**, 1460 (1987)
13. S.D. Brorson, A. Kazeroonian, J.S. Moodera, D.W. Face, T.K. Cheng, E.P. Ippen, M.S. Dresselhaus, G. Dresselhaus: Phys. Rev. Lett. **64**, 2172 (1990)
14. X.Y. Wang, D.M. Riffe, Y.S. Lee, M.C. Downer: Phys. Rev. B **50**, 8016 (1994)
15. R.W. Schoenlein, W.Z. Lin, J.G. Fujimoto, G.L. Eesley: Phys. Rev. Lett. **58**, 1680 (1987)
16. W.S. Fann, R. Storz, H.W.K. Tom, J. Bokor: Phys. Rev. B **46**, 13592 (1992)
17. Y.V. Afanasiev, O.N. Krokhin, G.V. Sklizkov: IEEE J. QE – **2** 483 (1966)
18. J.F. Ready: *Effects of High-Power Laser Radiation* (Academic, New York 1971)
19. V.A. Batanov, F.V. Bunkin, A.M. Prokhorov, V.B. Fedorov: Sov. Phys. –JETP **36**, 311 (1973)
20. A.M. Prokhorov, V.I. Konov, I. Ursu, I.N. Mihailescu: *Laser Heating of Metals* (Adam Hilger, Bristol 1990)
21. D. Strickland, G. Mourou: Opt. Commun. **56**, 219 (1985)
22. J.D. Kmetec, J.J. Macklin, J.F. Young: Opt. Lett. **16**, 1001 (1991)
23. S.I. Anisimov, M.I.Tribel'skii, Ya.G. Epel'baum: Sov. Phys. –JETP **51**, 802 (1980)